Journal of Building Engineering 91 (2024) 109704

Contents lists available at ScienceDirect

Journal of Building Engineering

journal homepage: www.elsevier.com/locate/jobe

Reactivity of air granulated basic oxygen furnace steel slag and its immobilization of heavy metals

Muhammad Jawad Ahmed [a,*], Katrin Schollbach [a], Sieger van der Laan [a,b], H.J. H. Brouwers [a]

[a] Department of Built Environment, Eindhoven University of Technology, Eindhoven, the Netherlands
[b] Tata Steel RD&T, Ceramics Research Centre, P.O. Box 10000, 1970 CA, IJmuiden, the Netherlands

ARTICLE INFO

Keywords:
Hydration products
Air granulation
Hydration degree
Immobilization of heavy metals

ABSTRACT

Air granulation of basic Oxygen furnace slag can improve its hydraulic potential to enhance recycling potential. The hydration behaviour of the slag has been investigated via isothermal calorimetry, QXRD, and TG/DTG analysis. The air granulated slag exhibited improved early-age hydration and led to the formation of C–S–H, hydrogarnet, and hydrotalcite phases. The slag reactivity is controlled by the dissolution of SiO_2 and Fe_2O_3 bearing phases as observed by SEM-EDX-based PARC analysis and the hydration degree reaches up to 41% after 28 days curing. The hydrated slag features an improved immobilization of V and Cr as confirmed by ICP-OES analysis.

1. Introduction

Basic oxygen furnace (BOF) slag is the byproduct of the basic oxygen converter steel-making slag. 90–110 kg of BOF slag is produced per ton of steel which accounts for 52.7% of the total steel furnace slags in Europe [1,2]. A small portion of BOF slag is partially recycled for low-end applications as aggregate for road base [3]. However, a significant amount of BOF slag is stored or landfilled [4], which conflicts with the goals of a circular economy. BOF slag contains a notable amount of C_2S (~35–45%) and C_4AF (~20–30%) [5], which have cementitious properties. However, the low reactivity and potential leaching of heavy metals (V and Cr) restrict its application as cement replacement [6–9].

Several strategies have been reported to enhance the recycling potential of BOF slag such as weathering, carbonation, mineral modification, high-temperature curing, and mechanical and chemical activation [10–15]. In addition to that, the BOF slag is added with other industrial byproducts such as fly ash, mine tailing, and blast furnace slag to valorize as fine aggregate as well as for the development of geopolymer-based materials [16–24]. But so far, no large-scale application for BOF slag as a binder has been reported. One way to enhance the reactivity of slag is fast cooling through granulation [25–29]. Granulation is a method already employed to enhance the blast furnace slag reactivity by preventing crystallization and generating amorphous content [30]. A previous study investigated the effect of air granulations on the mineralogical composition of BOF slag and concluded that the fast cooling of the slag did not generate a significant amorphous content. Instead, It impacted crystallite size and mineralogical composition [29,31]. The air granulation appears to suppress free lime formation, leading to a higher content of α'-C_2S compared to standard cooled BOF slag, and generated perovskite in addition to brownmillerite. Additionally, a higher Cr and V leaching (~300%, and ~640%, respectively, above the permissible legislative limit) was observed indicating that the air-granulated BOF slag exhibited a higher degree of dissolution of Cr and V bearing phases than standard cooled one [29]. Usually, the reaction products of the BOF slag are calcium silicate hydrate

* Corresponding author.
E-mail address: m.ahmed@tue.nl (M.J. Ahmed).

https://doi.org/10.1016/j.jobe.2024.109704
Received 22 March 2024; Received in revised form 20 May 2024; Accepted 20 May 2024
Available online 21 May 2024

(C–S–H), hydrogarnets, and hydrotalcite that tend to immobilize heavy metals especially potentially hazardous oxidation state V (V) and Cr (VI) in the hydration matrix [32]. Before applying this material, it is important to see if air granulated BOF slag can immobilize the heavy metals in the hydration matrix. Moreover, the high Cr and V leaching correlates with the high hydraulic activity in the air granulated BOF slag. Therefore, this study intends to follow up on this observation and investigate the hydraulic reactivity of air granulated BOF slag to determine if air granulation is a viable option to make the slag more reactive. This includes an investigation of the leaching behaviour because previous investigations on standard cooled BOF slag have shown that the hydration products of BOF slag tend to immobilize the Cr and V [33]. To the author's best knowledge, no systematic study about this topic exists yet.

This manuscript continues the work presented in an earlier paper [29] using the same air granulated slag. The two size fractions from 4-2- and 2-1-mm air granulated BOF slag were chosen as they yield ~90% of air granulation of the BOF slag to get representative insight. Early age hydration is investigated via isothermal calorimetry with a fixed water-to-solid (w/s) ratio while the later ages of 7-, 14-, and 28-days hydrated sample via quantitative X-ray diffraction (QXRD) and thermal gravimetric (TG) analysis. Furthermore, the microstructure of the 28-day hydrated sample has been analyzed through large-area phase mapping using SEM-EDS using phase recognition and characterization (PARC) analysis [34,35]. Moreover, the leaching of heavy metals (V and Cr specifically) in a 28-day hydrated slag sample has been quantified via ICP-OES and correlated with the degree of hydration.

2. Materials and methods

2.1. Materials

BOF slag is taken from regular production at Tata Steel Europe in Ijmuiden. The slag was poured in front of a strong fan for granulation at Harsco Metals Holland B.V. At the converter furnace the tap temperature was ~1592 °C with a batch size of 40 tonnes. It is known that approximately 40 °C drops occur in temperature at tapping. Further cooling of the slag can be neglected during transportation to the slag yard since the slag melt tends to develop a self-insulating freeze lining against the slag pot (Tata proprietary reports). Therefore, the temperature of BOF slag melt can be expected around 1550 °C, and 36 tonnes of the slag granulated with 4 tonnes remaining slag in the slag pot. It is difficult to measure the cooling rate during granulation and it depends on granule size. The larger granules take a longer time to cool and contain larger phenocrysts than the smaller ones. Because of these differences, the granulated BOF slag was sieved into several fractions in the lab. Most granules were in the range of 4–2 (49 wt%) and 2-1 mm (40 wt%) and free of any contamination of blast furnace slag [29]. To get a representative insight into air granulated BOF slag reactivity, the 4-2- and 2-1-mm fractions were chosen for the detailed hydration studies.

2.2. Methods

A representative sample was taken from every fraction of granulated converter slag. For this purpose, a static sample splitter was used. The 4-2-and-2-1 mm sieved air granulated BOF slag was then dried in an oven at 100 °C before grinding.

Two BOF slag fractions were ground for 40 min at 300 rpm to get fine particles via a planetary ball mill (Pulverisette 5, Fritsch). The specific density of the milled and 28-days hydrated slag was tested by a Helium pycnometer (AccuPyc II 1340). The specific densities of 4-2-and-2-1 mm slag are 3.63 cm^3/g. The PSD (particle size distribution) was determined using a Mastersizer 2000 from Malvern and the milled sample was dispersed in isopropanol. To understand the impact of specific surface area (SSA) on the hydration kinetics, the nitrogen adsorption (Tristar II 3020 V1.03 series micrometer) at 77 K was measured using BET (Brunauer-Emmett-Teller) methods. The PSD and SSA are shown in Fig. 1.

The influence of PSD and SSA on the hydraulic activity of the sample was analyzed with a TAM Air isothermal calorimeter at 20 °C for 96 h. The water-to-solid ratio (w/s) of 0.35 was used considering the low water demand of BOF slag. The slag powder was mixed with water *ex-situ* before calorimetric measurement.

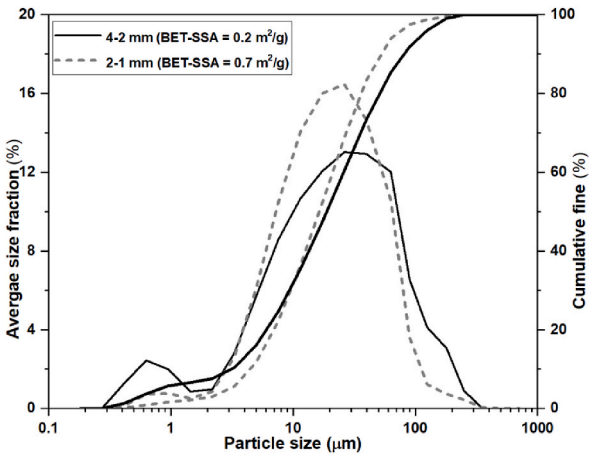

Fig. 1. The PSD (particle size distribution) of 4-2- and 2-1-mm fraction of air granulated BOF slag. In the inset, the specific surface area (SSA) obtained via the BET method is given.

Before XRF analysis, mass change was measured by heating slag samples at 1000 °C for 2 h. The chemical oxide composition of 4–2 and 2-1 mm of air granulated BOF slag was determined with X-ray fluorescence (XRF; PANalytical Epsilon 3, standardless) using fused beads as shown in Table 1. A gain on ignition (GOI) was observed due to the partial oxidation of ferrous oxide into ferric oxide.

X-ray powder diffractograms were acquired using a Bruker D2 and D4 diffractometer with an X-ray Co radiation X-ray source. The instrument has a fixed/variable divergence slit with an opening of 0.5° and 0.04 rad Soller slits. Reflections were measured between 5° and 90° 2 Theta (θ) with a step size of 0.02°. The 7-, 14-, and 28-days hydrated air granulated BOF slag samples were prepared with a 0.35 w/s ratio. The hydration of cured (7, 14, and 28 days old) samples was stopped via the solvent exchange (Isopropanol, Diethyl ether) method [36]. All samples for qualitative and quantitative analysis were backloaded in the sample holder for XRD measurement. The mineral phases were identified with X'Pert Highscore Plus 2.2 employing the ICDD PDF-2 database.

For QXRD, the 10 wt% silicon was added as an internal standard to quantify amorphous content. The samples were homogeneously mixed utilizing a McCrone micronizing mill. Quantification was done with TOPAS 4.2 software from Bruker. All crystal structures for quantification were obtained from the ICSD database. The error values given in the results are calculated by TOPAS.

TG (thermogravimetry) analysis was performed on the hydrated sample with a Jupiter STA 449 F1 (Netzsch) with heating of 15 °C/min under an N_2 atmosphere up to 1000 °C.

The 28-days hydrated samples of 2–1 -and 4-2 mm grains were embedded in resin (Struers EpoFix). The sample was polished against a flat surface without water. A spectral image (SI) was acquired with SEM-EDS on a carbon-coated sample using a beam current of 6.2 nA. One SI field consisted of a data set of 512 x 384 data points and took 20 min to acquire the data set. A JEOL JSM-7001 F SEM containing two 30 mm^2 SDD detectors (Thermo Fisher Scientific) and NORAN-System 7 hardware with NSS.3.3 software was applied with an accelerating voltage of 15 kV and a spot size of 1 μm. Several SI fields were measured to get a representative data set. The measured SI data set was evaluated for phase composition and distribution using Phase Recognition and Characterization (PARC) software developed by Tata Steel. Detailed information about PARC can be found elsewhere [35].

One batch leaching test was performed on a 28-days hydrated sample according to EN-12457 using deionized water with a liquid-to-solid (L/S) ratio of 10. The mixture was placed in plastic bottles and shaken continuously for 24 h at 21 ± 2 °C. After the experiment, the liquids were filtered through a 0.2 μm Polyether sulfone membrane and stored at 5 °C after acidifying with nitric acid (65% supra pure) to prevent precipitation. Before acidification, the pH was measured. An ICP-OES spectrometer (Spectroblue FMX36) was used for quantitative analysis of the leachate.

3. Results and discussion

3.1. Early age hydration

The early age (1–4 days) hydration behaviour of 4–2 mm and 2-1 mm fractions of air granulated BOF slag as well as standard cooled BOF slag has been investigated via isothermal calorimetry as shown in Fig. 2. The data is normalized by the mass of samples.

The 2-1 mm (0.7 m^2/g) fraction showed slightly higher heat of hydration (~2.2 mW/g, ~67 J/g) than the 4-2 mm fraction (0.2 m^2/g) (~2.0 mW/g, ~64 J/g) due to high specific surface area (SSA) after mechanical grinding. The obtained exothermic curve of the 2-1 mm fraction is directly comparable with the standard cooled BOF slag since both have a very similar specific surface area (0.7 m^2/g). The 2-1 mm fraction exhibited ~2.7 times higher heat release than the standard cooled BOF slag, a clear indicator that air granulation increased the reactivity of the slag (Fig. 2 (a)).

The main exothermic event in both air-granulated BOF slag samples can be attributed to the reactivity of calcium aluminoferrite phase such as brownmillerite that can be observed clearly in the 4-2 mm sample (Fig. 2 (a)) [37,38]. It appeared that the 4-2 mm fraction reacted earlier than the 2-1 mm sample which might be attributed to high percentage fines (D (10)) as shown in Fig. 1, despite the overall lower SSA after grinding. The exothermic peak appears around 8–12 h and is caused by the precipitation of C–S–H (calcium silicate hydrate). The narrow heat flux peak persists for 10–12 h which is consistent with the previous literature [39–44]. The early age reactivity of BOF slag is a serious parameter that restricts its application as a binder. Therefore, the standard cooled BOF slag is excluded in the subsequent ages (7, 14, and 28 days) hydration study as it is already well documented and outside the scope of this study [33,45].

3.2. Later age hydration

The air granulated BOF slag was hydrated, and mineralogical composition change was determined after 7, 14, and 28 d for both fractions via QXRD as shown in Fig. 3 (a, b). The detailed phase amounts with error, as well as the diffractogram with labeled peaks, can be found in Table S2, and Fig. S3 (a, b) respectively. Upon hydration, the crystalline phases decrease with time while the XRD amorphous content increases. The new crystalline phases evolved such as portlandite, hydroandradite ($Ca_3Fe_2(SiO_4)_{3-x}(OH)_{4x}$), and sjoegrenite ($Mg_6Fe_2(CO_3)(OH)_{16}$) in both slags' fractions.

It is evident that portlandite is the byproduct of the C_2S phase's reaction such as:

Table 1
Oxide (wt. %) composition of air granulated BOF slag.

Slag Fraction (mm)	MgO	Al_2O_3	SiO_2	P_2O_5	CaO	TiO_2	V_2O_5	Cr_2O_3	MnO	Fe_2O_3	GOI
2–1	8.3	3.4	14.8	1.2	44.9	1.4	0.6	0.2	4.2	20.8	0.2
4–2	8.2	4.1	14.4	1.2	44.9	1.4	0.6	0.2	4.2	20.6	0.3

GOI = Gain on ignition.

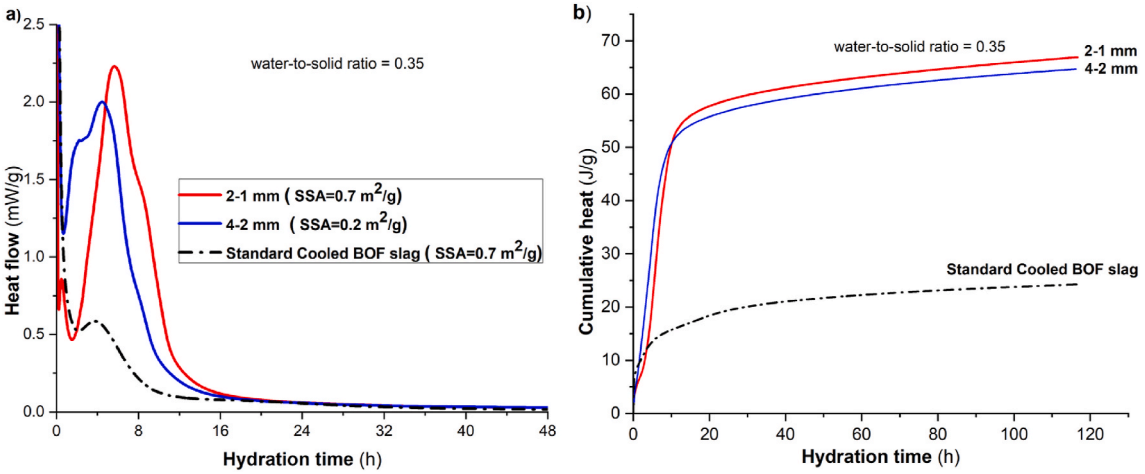

Fig. 2. The exothermic heat curve of 2-1- and 4-2 mm fraction of air granulated BOF slag (a) heat of hydration and (b) cumulative heat of hydration.

$$C_2S + 2H_2O \rightarrow 2Ca^{2+} + H_2SiO_4^{2-} + 2OH^- \quad \text{(A)}$$

In both slag fractions, the α′-C_2S as well as larnite crystalline content decreases (~22.1–11.7 wt%, ~22–13.3 wt% respectively) in 28 days of hydrated slag. The decrease in crystalline content of brownmillerite (~25.0–9.7 wt%), Fe, Mg-wüstite (~15.5–8.2 wt%), perovskite (~10.3–3.0 wt%) and increase in XRD amorphous (~7–41 wt%) content in the slag indicates the dissolution of the slag phases over time (Table S2, Fig. S3). The study indicates that the brownmillerite reaction will lead to the formation of hydrogarnet, Fe-hydroxide (amorphous), and portlandite. So far, we have not considered the formation of amorphous Fe-hydroxides except amorphous C–S–H (from slag hydration). Whether Fe could be a substitute for Al in the structure of the hydration products is still under investigation, but a decrease in the Al/Fe ratio significantly decreases the brownmillerite hydration [46]. In the presence of iron oxide and silica-rich system due to the dissolution of dicalcium silicate phases alongside Fe, Mg-wüstite, and perovskite, the brownmillerite favours the formation of Fe-katoite ($Ca_3Fe_2(OH)_{12}$) and hydroandradite ($Ca_3Fe_2(SiO_4)_{3\text{-}x}(OH)_{4x}$) as shown in B:

$$3Ca^{2+} + 2FeO_2^- + xHSiO_3^{2-} + xOH^- \rightarrow Ca_3Fe_2(SiO_4)_{3-x}(OH)_{4x} \quad \text{(B)}$$

The solubility product of hydroandradite decreases with increasing silica content in the solution leading to stabilization of the hydroandradite at room temperature. The amount of crystalline Fe-katoite + hydroandradite reaches 5.9 (2-1 mm) and 5.1 wt% (4-2 mm), respectively, after 28 days of hydration indicating the silica or iron oxide dissolution over time. Less than 1 wt% of the layered double hydroxide sjoegrenite ($Mg_6Fe_2(CO_3)(OH)_{16}$) was detected likely due to poor crystallinity of the phase.

To get more insight into the hydration product and XRD amorphous content, the TG/DTG thermogram of 7, 14, and 28 d hydrated slag fractions is shown in Fig. 4 (a, b). The mass loss events below ~60–200 °C can be assigned to the dehydration of C–S–H + sjoegrenite. The next mass loss events from ~260 to 400 °C can be attributed to the decomposition of silicious hydrogarnets [47–49]. It is important to mention here that the hydrotalcite phases start to decompose much earlier than the silicious hydrogarnet series (Fig. 4). The decomposition steps include the removal of interlayer water, dihydroxylation of brucite-like layers, and decarbonation. The decarbonation steps depend on the bond length of Fe–OH and Mg–OH bond length in the case of the hydrotalcite layer double hydroxide solid solution series. The increase in bond length lowers the decarbonation temperature [50,51]. The mass loss event ~440–520 °C and ~540–800 °C comprised of dehydration of portlandite as well as decarbonation of amorphous calcium carbonate and crystalline calcite respectively [52,53]. The 2-1 mm fraction of air granulated BOF slag exhibited a higher degree of volatiles than the 4-2 mm fraction after 28 d hydrated samples. The enhanced reactivity of the 2-1 mm fraction can be attributed to the higher SSA (0.7 m^2/g) than the 4-2 mm (0.2 m^2/g) fraction.

The QXRD and TGA are correlated to evaluate the degree of hydration (DOH) of both slag fractions. Firstly, the QXRD is rescaled considering the dilution effect and incorporation of bound water by using C:

$$W_{j,Rescaled,dilution\ corrected} = W_{j,Rietveld}(1 - Bound\ water_{TG}) \quad \text{(C)}$$

The bound water is calculated from TGA. Then, the DOH is calculated by employing D:

$$DOH(t) = 1 - W_{anhydrous,dilution\ corrected}(t) / W_{anhydrous}(t=0) \quad \text{(D)}$$

W_j = weight of XRD phases (wt. %)

Bound $water_{TG}$ = (mass loss $_{(104-1000\ °C)}$ − calcite)

The 2-1 mm slag fraction exhibited higher (~18%) DOH than 4-2 mm (~15%) after 7 days of hydration as shown in Fig. 5. A slight

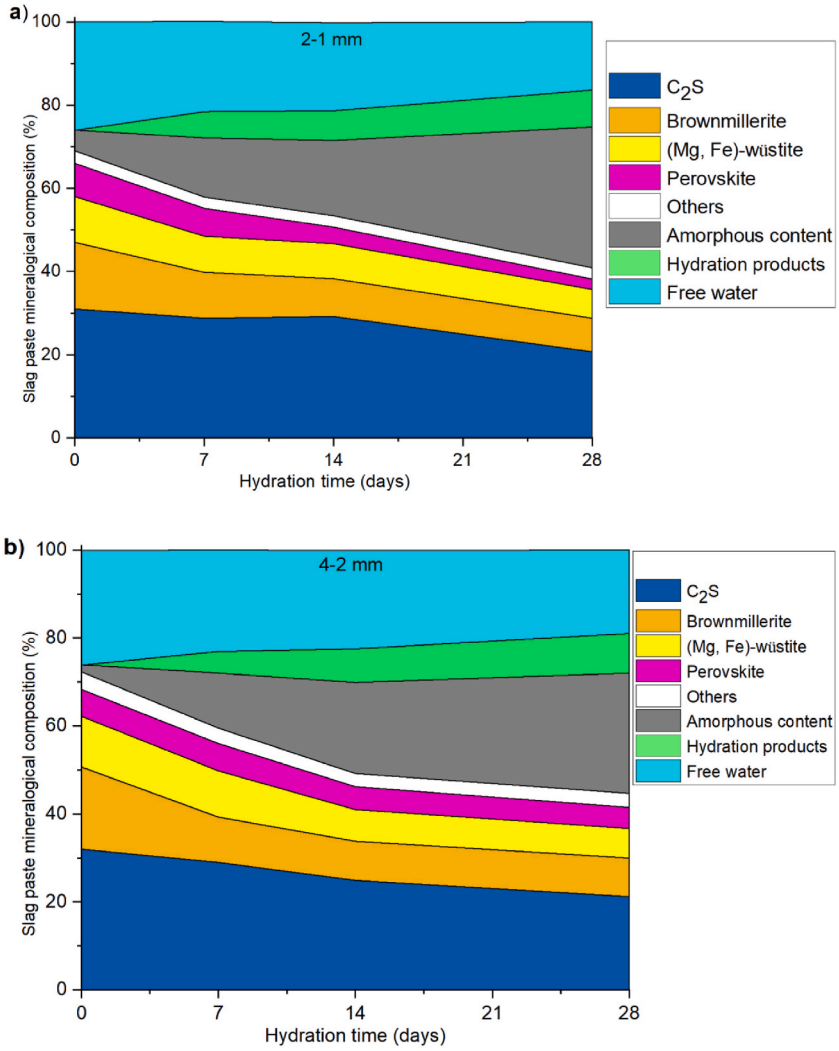

Fig. 3. QXRD of a) 2-1- and b) 4-2-mm fraction of hydrated air granulated BOF slag cured for 7, 14, and 28 days. Free water value is taken from the initial water-to-solid ratio and bound water is calculated from the loss on ignition at (50–550 °C). The term "hydration product" is used for all crystalline hydration products such as hydroandradite + katoite, portlandite, and pyroaurite/sjoegrenite.

increase in DOH (~18–21%) is observed from 7 to 14 days for 2-1 mm indicating the slag's slow reactivity at this time while the 4-2 mm slag fraction keeps reacting and reaches ~27%. After 28 days of hydration, 2-1 mm fraction exhibited higher overall DOH (41%) than 4-2 mm (36%) can be attributed to the high SSA of 2–1 mm slag fraction. The DOH and TG bound water (mass loss) are significantly higher than standard cooled BOF slag which indicates the high reactivity of the slag [54].

To study the influence of air granulated hydration on the microstructure, the SEM-EDX-based large area phase mapping was carried out on 28 days of hydrated 2–1 and 4-2 mm air granulated slag fraction using PARC software as shown in Fig. 6 (a, b) (see Fig. S4 for 28 d hydrated 4-2 mm fraction) [55]. It is clear from the PARC image that the 2-1 mm slag fraction contained large crystals of C_2S and (Mg, Fe)O embedded in a fine-grained matrix. The fine-grained matrix or matrix phase is a mix of different mineral phases with a size below the EDX resolution of 1 μm [29]. Based on their composition they were divided into 3 parts: Matrix CS (Ca, Si rich), CF (Ca, Fe rich), and MF (Mg, Fe rich) (see Ref. [29] for further details).

Contrary to XRD analysis, the C_2S polymorphs (α', β) cannot be differentiated as they have the same chemical composition. The C_2S phase also exhibited the presence of several minor ions such as P_2O_5, Cr_2O_3, V_2O_5, Fe_2O_3, TiO_2, etc. which tend to occupy more Si sites according to structure difference factor (D) calculations [56]. It is important to mention here that a significant amount of V_2O_5 and P_2O_5 are incorporated into the crystal structure of C_2S while the detection of Cr_2O_3 is erroneous due to a sum peak of Ca + Si═Cr in the EDS spectrum [57,58]. However, the EPMA analysis revealed that the C_2S contains Cr_2O_3 <0.05 wt% [57]. The "hydration product" phase is a heterogeneous mix of the crystalline and amorphous hydration products detected with XRD and TG that cannot be differentiated with SI due to their size below the spatial resolution of EDS. The phase named "Portlandite" also contains calcium hydroxide and carbonate, as both are present according to TG and XRD, however, they are difficult to recognize with EDX. The

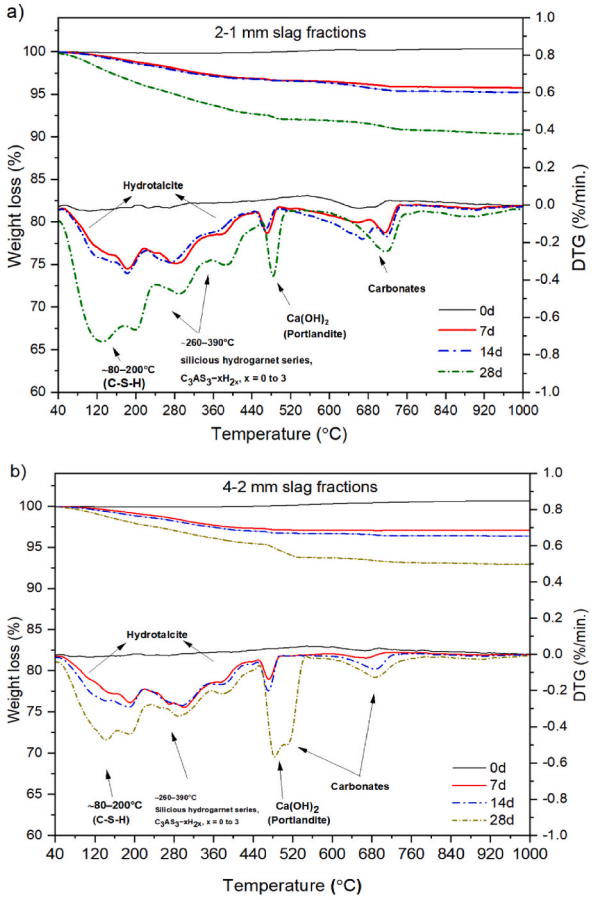

Fig. 4. Thermal gravimetric analysis of hydrated air granulated BOF slag fractions a) 2-1 mm fraction and 1st derivative of thermal gravimetric analysis of 2–1 mm fractions b) 4-2 mm fractions and 1st derivative of thermal gravimetric analysis of 4–2 mm fraction.

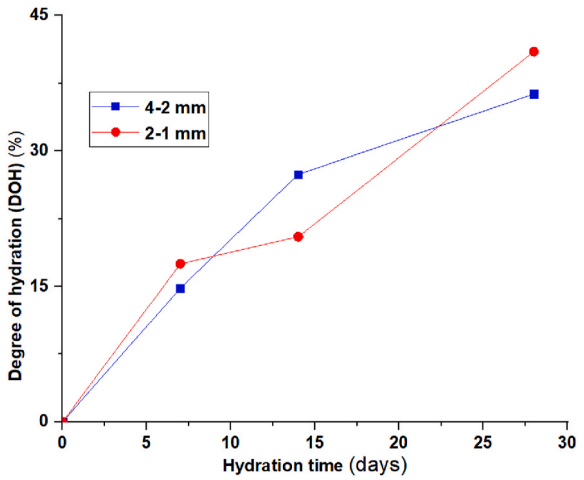

Fig. 5. 2-1-and 4-2 mm fraction of hydrated air granulated BOF slag cured for 7, 14, and 28 days.

hydrated sample microstructure was divided into hydration products, C_2S phases, portlandite, wüstite, matrix CS (CaSi), CF (CaFe), and MF(MgFe) according to Ca/Si, Ca/Fe and Mg/Fe, etc. composition by using a density plot as shown in Fig. 6 (b) [29,45,59].

The area% of each phase and oxide composition of the hydrated 2-1 mm slag fraction is presented in Table 2 (see Table S5 4-2 mm fractions). The hydration product takes up ~49 area% of the total. The calcium to silica and calcium to iron oxide ratio in the hydration

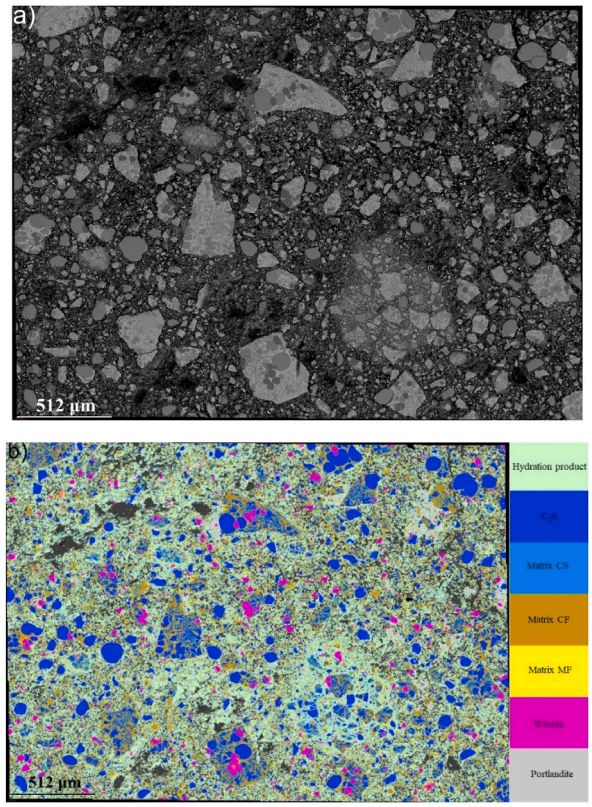

Fig. 6. Microstructure analysis of 1–2 mm fraction of air granulated BOF slag after 28 days of hydration at 512 µm a) backscattered image (BSI) b) PARC phase map.

product is ~2, and 3.4, respectively, indicating the dissolution of dicalcium silicate as well as iron oxide bearing brownmillerite phases.

3.3. Environmental behaviour of hydrated slag

The one batch leaching test was performed on the 28 days hydrated 2-1 mm and 4-2 mm air granulated BOF slag fractions as shown in Table 3 and compared to the leaching on the slag granulated BOF slag before the milling and hydration. The data for unhydrated slag was published previously and used for direct comparison [29]. One can argue that a direct comparison cannot be made due to the dilution effect of the bound water in slag. As the 28 days hydrated 2-1- and 4-2-mm slag has a low value of loss on ignition (LOI) (~8 and 6 wt% respectively), the dilution effect will not cause much change in elemental composition.

The vanadium element leaching decreases from ~11.03 to 1.3 mg/kg for the 2-1 mm fraction after 28 days of hydration and from ~11.83 to 1.1 mg/kg for the 4-2 mm slag fraction. These vanadium emission (~1.1–1.3 mg/kg) values are below the permissible (~1.8 mg/kg) emission values. Cr emission decreases from ~1.86 to 0.72 and from 1.75 to 1.01 mg/kg, respectively, in 2-1- and 4-2-mm slag fraction which is above the permissible emission (0.63 mg/kg) values. The remaining heavy metals are below the legal limits of the Dutch soil quality decree.

The pH of the hydrated slag sample lies in the range of 11.5–11.8. The equilibrium formation of Ca–Si–H phases with C_2S dissolution would permit the high Ca^{2+} concentration in the leachate which limits the solubility of vanadium oxide [60]. From the PARC analysis of the 2-1- and 4-2-mm slag granules, it was concluded that the C_2S contributes more toward V leaching in the slag. Therefore, the V is immobilized in the hydration product phase upon C_2S reactivity as C–S–H actively takes V_2O_5 on the tetrahedral Si-site. All these factors contribute toward the immobilization of V in the BOF slag.

Table 2
Phases identified in 28 days hydrated 2-1 mm granulated slag in area % via PARC analysis.

2-1 mm slag	Phases Amount (Area%)	MgO	Al_2O_3	SiO_2	P_2O_5	CaO	TiO_2	V_2O_5	Cr_2O_3	MnO	Fe_2O_3
Hydration Products	48.8	5.7	1.8	23.5	1.9	46.8	1.4	0.7	0.5	2.9	13.9
C_2S	25.5	0.7	0.3	30.1	2.9	61.1	1	0.4	1.3	0.2	1.9
Matrix	21.3	6.3	3.1	7.4	0.6	36.2	2.5	0.8	0.3	6.7	35.6
Wuestite	2.8	67.2	0	1.6	0	2.2	0.1	0.2	0.4	8.2	20
Portlandite	1.4	0.3	0.2	1.2	0.3	94.5	0.7	0	0.1	0.5	1.7
Bulk PARC Composition		16.1	1.1	12.8	1.1	48.1	1.1	0.4	0.5	3.7	14.6

Table 3
The heavy metals leaching values 1–2 mm and 2–4 mm of air granulated slag fraction. (The leaching values higher than the permissible limit are indicated in bold numbers).

Slag fractions	Units	Permissible limit	Unhydrated 2–1 mm	28 days hydrated 2–1 mm	Unhydrated 4–2 mm	28 days hydrated 4–2 mm
pH (20 ± 2°C)			10.8	11.5	11	11.8
Antimony (Sb)	mg/kg	0.32	0.19	L.D.	0.19	L.D.
Arsenic (As)	mg/kg	0.9	0.22	L.D.	0.21	L.D.
Barium (Ba)	mg/kg	22	0.02	0.1	0.11	0.6
Chromium (Cr)	mg/kg	0.63	**1.86**	**0.72**	**1.75**	**1.01**
Vanadium (V)	mg/kg	1.8	**11.03**	1.3	**11.83**	1.1

L.D. = below detection limit.

In the case of Cr leaching, the identifiable Cr complex is $CaCrO_4$ at pH ~11.5–11.9 as shown:

$$Ca^{2+} + CrO_4^{2-} \leftrightharpoons CaCrO_4 \quad \text{(E)}$$

The $CaCrO_4$ is a soluble species in aqueous media, and the decrease in the Cr leaching can be attributed to the heavy metal immobilization potential of the hydration product particularly hydrogarnet and layered double hydroxide which can host large quantities of Cr^{6+} [61]. It is worth mentioning here that the BOF slag contains Cr^{3+} in brownmillerite and wüstite-type phases [62,63].

Consequently, the 28 days hydrated 2-1 mm slag sample shows a higher decrease (~61%) in Cr-leaching than (~42%) 4-2 mm slag sample due to high DOH (~41%) value (Table 3, Fig. 6). In summary, the Cr and V can be immobilized in the slag matrix by enhancing slag hydration via increasing the reactivity of C_2S and brownmillerite phases.

As compared to standard cooled BOF slag, the overall higher leaching of the air-granulated BOF slag might be due to a higher oxidation state of V and Cr since the air-granulated slag is more oxidized overall. However, further investigation will be required to confirm it.

4. Conclusions

The hydration of air granulated BOF slag fractions 2-1-and-4-2 mm as well as the immobilization behaviour of Cr and V, has been investigated.

The early age reactivity of air-granulated slag depends on the specific surface area (SSA). The air-granulated slag exhibited a significantly (~2.7 times) higher reactivity than the standard cooled BOF slag. The hydration products consisted of C–S–H, a mix of Fe-katoite and hydroandradite, layered double hydroxide (sjoegrenite), and portlandite. The formation of hydration products is controlled by the dissolution of C_2S and brownmillerite which are very similar to the reaction of standard cooled BOF slag.

The calculated reaction degree shows that the 2-1 mm fraction exhibited higher DOH (~41%) than the 4-2 mm (36%) fraction after 28 days of hydration. The high reactivity of 2–1 mm slag is attributed to higher SSA (0.7 m^2/g) than the 4-2 mm (0.2 m^2/g) slag fraction.

PARC analysis of 28 days hydrated 2-1 mm slag fraction confirms that the hydration product takes up ~49 area% in total. The calcium to silica and calcium to iron oxide ratio in the hydration product is ~2, and 3.4, respectively, indicating the dissolution of dicalcium silicate as well as iron oxide bearing brownmillerite phases.

The 2-1- and -4-2-mm slag fractions after 28 days of hydration immobilize up to ~88% and ~91% of vanadium respectively as compared to the unhydrated slag. The 28-day hydrated 2-1 mm slag fraction immobilizes Cr up to ~61% due to high DOH (~41%) while the hydrated 2–4 mm slag fraction decreases Cr leaching up to ~42%. The decrease in the V and Cr leaching is largely attributed to immobilization in hydration products.

In summary, a current study provides detailed insight into the hydration of air granulated BOF slag. This study shows that the air granulation shows the promise of high reactivity at an early stage alongside immobilizing Cr and V in the hydration product which confirms the fitness of the material for sustainable building products. The efforts like mechano-chemical activation, and partial replacement with other industrial byproducts can enhance its recycling potential for the valorization of the steel slag which will be the next step of this study.

CRediT authorship contribution statement

Muhammad Jawad Ahmed: Writing – original draft, Methodology, Investigation, Formal analysis, Data curation, Conceptualization. **Katrin Schollbach:** Writing – review & editing, Validation, Software, Resources, Project administration, Formal analysis, Conceptualization. **Sieger van der Laan:** Writing – review & editing, Visualization, Validation, Supervision, Software, Project administration, Formal analysis. **H.J.H. Brouwers:** Writing – review & editing, Supervision, Resources, Project administration, Funding acquisition.

Declaration of competing interest

The authors declare that they have no known competing financial interests or personal relationships that could have appeared to influence the work reported in this paper.

Data availability

Data will be made available on request.

6. Acknowledgment

The authors would like to acknowledge the financial support by NWO (The Netherlands Organisation for Scientific Research) for funding this research (project no.10023338) and M2i (Materials Innovation Institute, project no. S81.6.15565b) for managing this project. The authors would like to extend a special thanks to Winnie F. Santos (TU Eindhoven, the Netherlands) for generously sharing data on standard cooled BOF slag. Furthermore, the authors wish to express their gratitude to the following sponsors of this research: Tata Steel; ENCI; V.d. Bosch Beton; Blue Phoenix Group; Hess.

Appendix A. Supplementary data

Supplementary data to this article can be found online at https://doi.org/10.1016/j.jobe.2024.109704.

References

[1] A.M. Kaja, K. Schollbach, S. Melzer, S.R. van der Laan, H.J.H. Brouwers, Q. Yu, Hydration of potassium citrate-activated BOF slag, Cement Concr. Res. 140 (2021) 106291, https://doi.org/10.1016/j.cemconres.2020.106291.
[2] K. Horii, N. Tsutsumi, Y. Kitano, T. Kato, Processing and reusing technologies for steelmaking slag, Nippon Steel Tech. Rep. (2013).
[3] L. De Windt, P. Chaurand, J. Rose, Kinetics of steel slag leaching: batch tests and modeling, Waste Manag. 31 (2011) 225–235, https://doi.org/10.1016/j.wasman.2010.05.018.
[4] J. Guo, Y. Bao, M. Wang, Steel slag in China: treatment, recycling, and management, Waste Manag. (2018), https://doi.org/10.1016/j.wasman.2018.04.045.
[5] S.Z. Carvalho, F. Vernilli, B. Almeida, M. Demarco, S.N. Silva, The recycling effect of BOF slag in the portland cement properties, Resour. Conserv. Recycl. 127 (2017) 216–220, https://doi.org/10.1016/J.RESCONREC.2017.08.021.
[6] Q. Alam, K. Schollbach, C. van Hoek, S. van der Laan, T. de Wolf, H.J.H.J.H. Brouwers, Q. Alam, C. van Hoek, S. van der Laan, T. de Wolf, H.J.H.J.H. Brouwers, K. Schollbach, C. van Hoek, S. van der Laan, T. de Wolf, H.J.H.J.H. Brouwers, In-depth mineralogical quantification of MSWI bottom ash phases and their association with potentially toxic elements, Waste Manag. submitted (2019) 1–12, https://doi.org/10.1016/j.wasman.2019.01.031.
[7] P. Chaurand, J. Rose, V. Briois, L. Olivi, J.L. Hazemann, O. Proux, J. Domas, J.Y. Bottero, Environmental impacts of steel slag reused in road construction: a crystallographic and molecular (XANES) approach, J. Hazard Mater. (2007), https://doi.org/10.1016/j.jhazmat.2006.02.060.
[8] S. Teir, S. Eloneva, C.J. Fogelholm, R. Zevenhoven, Dissolution of steelmaking slags in acetic acid for precipitated calcium carbonate production, Energy 32 (2007) 528–539, https://doi.org/10.1016/J.ENERGY.2006.06.023.
[9] A.M. Kaja, A. Delsing, S.R. van der Laan, H.J.H. Brouwers, Q. Yu, Effects of carbonation on the retention of heavy metals in chemically activated BOF slag pastes, Cement Concr. Res. 148 (2021) 106534, https://doi.org/10.1016/j.cemconres.2021.106534.
[10] A.C.P. Martins, J.M. Franco de Carvalho, L.C.B. Costa, H.D. Andrade, T.V. de Melo, J.C.L. Ribeiro, L.G. Pedroti, R.A.F. Peixoto, Steel slags in cement-based composites: an ultimate review on characterization, applications and performance, Construct. Build. Mater. 291 (2021), https://doi.org/10.1016/j.conbuildmat.2021.123265.
[11] H. Wulfert, H.M. Ludwig, G. Wimmer, A new process for production of cement clinker from steelmaking slags, Cem. Int. (2017).
[12] Y. Wang, P. Suraneni, Experimental methods to determine the feasibility of steel slags as supplementary cementitious materials, Construct. Build. Mater. 204 (2019) 458–467, https://doi.org/10.1016/j.conbuildmat.2019.01.196.
[13] L. Kriskova, Y. Pontikes, Ö. Cizer, G. Mertens, W. Veulemans, D. Geysen, P.T. Jones, L. Vandewalle, K. Van Balen, B. Blanpain, Effect of mechanical activation on the hydraulic properties of stainless steel slags, Cement Concr. Res. (2012), https://doi.org/10.1016/j.cemconres.2012.02.016.
[14] T.H. Lu, Y.L. Chen, P.H. Shih, J.E. Chang, Use of basic oxygen furnace slag fines in the production of cementitious mortars and the effects on mortar expansion, Construct. Build. Mater. 167 (2018) 768–774, https://doi.org/10.1016/j.conbuildmat.2018.02.102.
[15] J. Feng, J. Sun, A comparison of the 10-year properties of converter steel slag activated by high temperature and an alkaline activator, Construct. Build. Mater. 234 (2020) 116948, https://doi.org/10.1016/j.conbuildmat.2019.116948.
[16] F. Saly, L. Guo, R. Ma, C. Gu, W. Sun, Properties of steel slag and stainless steel slag as cement replacement materials: a comparative study, J. Wuhan Univ. Technol. Sci. 336 (33) (2018) 1444–1451, https://doi.org/10.1007/S11595-018-1989-3, 2018.
[17] T. Mashifana, N. Sithole, Utilization of fly ash: basic oxygen furnace slag as a raw material in geopolymerization, IOP Conf. Ser. Mater. Sci. Eng. 652 (2019) 012060, https://doi.org/10.1088/1757-899X/652/1/012060.
[18] N.T. Sithole, F. Okonta, F. Ntuli, Development of lightweight construction blocks by alkaline activation of bof slag, J. Solid Waste Technol. Manag. 45 (2019) 175–185, https://doi.org/10.5276/JSWTM/2019.175.
[19] N.T. Sithole, F. Okonta, F. Ntuli, Mechanical properties and structure of fly ash modified basic oxygen furnace slag based geopolymer masonry blocks, J. Solid Waste Technol. Manag. 46 (2020) 372–383, https://doi.org/10.5276/JSWTM/2020.372.
[20] S. Sandybay, C.S. Shon, A. Tukaziban, D. Syzdykov, I. Orynbassarov, D. Zhang, J.R. Kim, Blended basic oxygen furnace (BOF) slag with ground granulated blast furnace slag (GGBFS) as a pozzolanic material, Mater. Sci. Forum 1053 (2022) 331–337, https://doi.org/10.4028/P-Q7N2CU.
[21] T. Mashifana, J. Sebothoma, T. Sithole, Alkaline activation of basic oxygen furnace slag modified gold mine tailings for building material, Adv. Civ. Eng. 2021 (2021), https://doi.org/10.1155/2021/9984494.
[22] J.C.O. Zepper, S.R. van der Laan, K. Schollbach, H.J.H. Brouwers, Reactivity of BOF slag under autoclaving conditions, Construct. Build. Mater. 364 (2023) 129957, https://doi.org/10.1016/j.conbuildmat.2022.129957.
[23] M.J. Ahmed, S. Durand, M. Antoun, F. Gauvin, S. Amziane, H.J.H. Brouwers, Utilization of air granulated basic oxygen furnace slag as a binder in belite calcium sulfoaluminate cement: a sustainable alternative, J. Clean. Prod. 436 (2024) 140539, https://doi.org/10.1016/J.JCLEPRO.2023.140539.
[24] M. Jawad Ahmed, W. Franco Santos, H.J.H. Brouwers, Air granulated basic Oxygen furnace (BOF) slag application as a binder: effect on strength, volumetric stability, hydration study, and environmental risk, Construct. Build. Mater. 367 (2023) 130342, https://doi.org/10.1016/j.conbuildmat.2023.130342.
[25] P. Yu, S. Wang, Y. Li, G. Xu, A review of granulation process for blast furnace slag, MATEC Web Conf. (2016), https://doi.org/10.1051/matecconf/20166806007.

[26] F. Engström, D. Adolfsson, Q. Yang, C. Samuelsson, B. Björkman, Crystallization behaviour of some steelmaking slags, Steel Res. Int. 81 (2010) 362–371, https://doi.org/10.1002/SRIN.200900154.

[27] M. Loncnar, M. Zupančič, P. Bukovec, A. Jaklič, The effect of water cooling on the leaching behaviour of EAF slag from stainless steel production, Mater. Tehnol. (2009).

[28] D. Durinck, P.T. Jones, B. Blanpain, P. Wollants, Air-cooling of metallurgical slags containing multivalent oxides, J. Am. Ceram. Soc. 91 (2008) 3342–3348, https://doi.org/10.1111/j.1551-2916.2008.02597.x.

[29] K. Schollbach, M.J. Ahmed, S.R. van der Laan, The mineralogy of air granulated converter slag, Int. J. Ceram. Eng. Sci. 3 (2021) 21–36, https://doi.org/10.1002/ces2.10074.

[30] S.K. Tripathy, J. Dasu, Y.R. Murthy, G. Kapure, A.R. Pal, L.O. Filippov, Utilisation perspective on water quenched and air-cooled blast furnace slags, J. Clean. Prod. 262 (2020) 121354, https://doi.org/10.1016/j.jclepro.2020.121354.

[31] N.Y. Mostafa, S.A.S. El-Hemaly, E.I. Al-Wakeel, S.A. El-Korashy, P.W. Brown, Hydraulic activity of water-cooled slag and air-cooled slag at different temperatures, Cement Concr. Res. 31 (2001) 475–484, https://doi.org/10.1016/S0008-8846(00)00462-2.

[32] H. Miyata, K. Fujii, T. Ono, Y. Kubokawa, T. Ohno, F. Hatayama, Fourier-transform infrared investigation of structures of vanadium oxide on various supports, J. Chem. Soc. Faraday Trans. 1 Phys. Chem. Condens. Phases. 83 (1987) 675, https://doi.org/10.1039/f19878300675.

[33] W.F. Santos, K. Schollbach, S. Melzer, S.R. van der Laan, H.J.H. Brouwers, Quantitative analysis and phase assemblage of basic oxygen furnace slag hydration, J. Hazard Mater. (2023) 131029, https://doi.org/10.1016/J.JHAZMAT.2023.131029.

[34] C. van Hoek, J. Small, S. van der Laan, Large-area phase mapping using PhAse recognition and characterization (PARC) software, micros, Today Off. 24 (2016) 12–21, https://doi.org/10.1017/S1551929516000572.

[35] K. Schollbach, S. van der Laan, in: Ind Waste (Ed.), Chapter 3 Microstructure Analysis with Quantitative Phase Mapping Using SEM-EDS and Phase Recognition and Characterization (PARC) Software: Applied to Steelmaking Slag, De Gruyter, 2021, pp. 57–96, https://doi.org/10.1515/9783110674941-003.

[36] Sc Karen L, S. Ruben, L. Barbara, A Practical Guide to Microstructural Analysis of Cementitious Materials, CRC Press, Boca Raton, 2016.

[37] T. Hertel, J. Neubauer, F. Goetz-Neunhoeffer, Study of hydration potential and kinetics of the ferrite phase in iron-rich CAC, Cement Concr. Res. 83 (2016) 79–85, https://doi.org/10.1016/j.cemconres.2016.01.004.

[38] Q. Wang, P. Yan, S. Han, The influence of steel slag on the hydration of cement during the hydration process of complex binder, Sci. China Technol. Sci. 54 (2011) 388–394, https://doi.org/10.1007/s11431-010-4204-0.

[39] T. Zhang, Q. Yu, J. Wei, J. Li, Investigation on mechanical properties, durability and micro-structural development of steel slag blended cements, J. Therm. Anal. Calorim. 110 (2012) 633–639, https://doi.org/10.1007/s10973-011-1853-6.

[40] S. Zhuang, Q. Wang, Inhibition mechanisms of steel slag on the early-age hydration of cement, Cement Concr. Res. 140 (2021) 106283, https://doi.org/10.1016/j.cemconres.2020.106283.

[41] W. Nocuń-Wczelik, Differential calorimetry as a tool in the studies of cement hydration kinetics with sulphate and nitrate solutions, J. Therm. Anal. Calorim. 130 (2017) 249–259, https://doi.org/10.1007/s10973-017-6378-1.

[42] E. Dubina, L. Black, R. Sieber, J. Plank, Interaction of water vapour with anhydrous cement minerals, Adv. Appl. Ceram. 109 (2010) 260–268, https://doi.org/10.1179/174367509X12554402491029.

[43] J. Li, Q. Yu, J. Wei, T. Zhang, Structural characteristics and hydration kinetics of modified steel slag, Cement Concr. Res. 41 (2011) 324–329, https://doi.org/10.1016/j.cemconres.2010.11.018.

[44] M.J. Ahmed, K. Lambrechts, X. Ling, K. Schollbach, H.J.H. Brouwers, Effect of hydroxide, carbonate, and sulphate anions on the β-dicalcium silicate hydration rate, Cement Concr. Res. 173 (2023) 107302, https://doi.org/10.1016/j.cemconres.2023.107302.

[45] A.M. Kaja, S. Melzer, H.J.H. Brouwers, Q. Yu, On the optimization of BOF slag hydration kinetics, Cem. Concr. Compos. 124 (2021) 104262, https://doi.org/10.1016/j.cemconcomp.2021.104262.

[46] X. Huang, F. Wang, S. Hu, Y. Lu, M. Rao, Y. Mu, Brownmillerite hydration in the presence of gypsum: the effect of Al/Fe ratio and sulfate ions, J. Am. Ceram. Soc. 102 (2019) 5545–5554, https://doi.org/10.1111/jace.16384.

[47] P.A. Terry, Characterization of Cr ion exchange with hydrotalcite, Chemosphere 57 (2004) 541–546, https://doi.org/10.1016/j.chemosphere.2004.08.006.

[48] N. Noguchi, K. Siventhirarajah, T. Chabayashi, H. Kato, T. Nawa, Y. Elakneswaran, Hydration of ferrite-rich Portland cement: evaluation of Fe-hydrates and Fe uptake in calcium-silicate-hydrates, Construct. Build. Mater. 288 (2021) 123142, https://doi.org/10.1016/j.conbuildmat.2021.123142.

[49] B.Z. Dilnesa, E. Wieland, B. Lothenbach, R. Dähn, K.L. Scrivener, Fe-containing phases in hydrated cements, Cement Concr. Res. 58 (2014) 45–55, https://doi.org/10.1016/j.cemconres.2013.12.012.

[50] K. Rozov, U. Berner, C. Taviot-Gueho, F. Leroux, G. Renaudin, D. Kulik, L.W. Diamond, Synthesis and characterization of the LDH hydrotalcite–pyroaurite solid-solution series, Cement Concr. Res. 40 (2010) 1248–1254, https://doi.org/10.1016/j.cemconres.2009.08.031.

[51] G. Yu, Y. Zhou, R. Yang, M. Wang, L. Shen, Y. Li, N. Xue, X. Guo, W. Ding, L. Peng, Dehydration and dehydroxylation of layered double hydroxides: new insights from solid-state NMR and FT-IR studies of deuterated samples, J. Phys. Chem. C 119 (2015) 12325–12334, https://doi.org/10.1021/acs.jpcc.5b01449.

[52] N. Vogler, P. Drabetzki, M. Lindemann, H.-C. Kühne, Description of the concrete carbonation process with adjusted depth-resolved thermogravimetric analysis, J. Therm. Anal. Calorim. 147 (2022) 6167–6180, https://doi.org/10.1007/s10973-021-10966-1.

[53] I.E. Teune, K. Schollbach, M.V.A. Florea, H.J.H. Brouwers, Carbonation of hydrated cement: the impact of carbonation conditions on CO2 sequestration, phase formation, and reactivity, J. Build. Eng. 79 (2023) 107785, https://doi.org/10.1016/J.JOBE.2023.107785.

[54] W.F. Santos, K. Schollbach, S. Melzer, S.R. van der Laan, H.J.H. Brouwers, Quantitative analysis and phase assemblage of basic oxygen furnace slag hydration, J. Hazard Mater. 450 (2023) 131029, https://doi.org/10.1016/j.jhazmat.2023.131029.

[55] C. van Hoek, J. Small, S. van der Laan, Large-area phase mapping using PhAse R ecognition and characterization (PARC) software, micros, Today Off. 24 (2016) 12–21, https://doi.org/10.1017/s1551929516000572.

[56] Z. Wensheng, R. Xuehong, O. Shixi, 硅 酸 盐 学 报 Development on Ion Substitution Effect on the Crystal Structure and Properties of Tricalcium Silicate, (n.d.). doi:10.14062/j.issn.0454-5648.2011.10.023..

[57] A.M. Kaja, A. Delsing, S.R. van der Laan, H.J.H. Brouwers, Q. Yu, Effects of carbonation on the retention of heavy metals in chemically activated BOF slag pastes, Cement Concr. Res. 148 (2021) 106534, https://doi.org/10.1016/J.CEMCONRES.2021.106534.

[58] C. Liu, S. Huang, P. Wollants, B. Blanpain, M. Guo, Valorization of BOF steel slag by reduction and phase modification: metal recovery and slag valorization, Metall. Mater. Trans. B 48 (2017) 1602–1612, https://doi.org/10.1007/s11663-017-0966-0.

[59] S.R. Van Der Laan, K. Schollbach, T. Steel, Reactivity of BOF Slag under Autoclaving Conditions, 1970.

[60] M.J. Ahmed, R. Cuijpers, K. Schollbach, S. Van Der Laan, M. Van Wijngaarden-Kroft, T. Verhoeven, H.J.H. Brouwers, V and Cr substitution in dicalcium silicate under oxidizing and reducing conditions – synthesis, reactivity, and leaching behavior studies, J. Hazard Mater. 442 (2023) 130032, https://doi.org/10.1016/j.jhazmat.2022.130032.

[61] E. Rodrigues, O. Almeida, H. Brasil, D. Moraes, M.A.L. dos Reis, Adsorption of chromium (VI) on hydrotalcite-hydroxyapatite material doped with carbon nanotubes: equilibrium, kinetic and thermodynamic study, Appl. Clay Sci. 172 (2019) 57–64, https://doi.org/10.1016/j.clay.2019.02.018.

[62] A.-M. Fällman, Leaching of chromium and barium from steel slag in laboratory and field tests — a solubility controlled process? Waste Manag. 20 (2000) 149–154, https://doi.org/10.1016/S0956-053X(99)00313-X.

[63] E. Kim, J. Spooren, K. Broos, L. Horckmans, M. Quaghebeur, K.C. Vrancken, Selective recovery of Cr from stainless steel slag by alkaline roasting followed by water leaching, Hydrometallurgy 158 (2015) 139–148, https://doi.org/10.1016/j.hydromet.2015.10.024.